Chemical Engineering Journal 270 (2015) 282–289

Contents lists available at ScienceDirect

Chemical Engineering Journal

journal homepage: www.elsevier.com/locate/cej

A supported Cu(I)@MIL-100(Fe) adsorbent with high CO adsorption capacity and CO/N_2 selectivity

Junjie Peng [a], Sikai Xian [a], Jing Xiao [b,*], Yan Huang [a], Qibin Xia [b], Haihui Wang [a], Zhong Li [a,*]

[a] School of Chemistry and Chemical Engineering, South China University of Technology, Guangzhou 510640, PR China
[b] The Key Laboratory of Enhanced Heat Transfer and Energy Conversation Ministry of Education, South China University of Technology, Guangzhou 510640, PR China

HIGHLIGHTS

- A novel Cu(I)@MIL-100(Fe) was successfully synthesized.
- Cu(I)@MIL-100(Fe) exhibits a high CO adsorption capacity of 2.78 mmol/g.
- CO/N_2 adsorption selectivity of 0.8Cu(I)@MIL-100(Fe) was as high as 169.
- The isosteric heat of CO over 0.8Cu(I)@MIL-100(Fe) was ~50 kJ/mol.

GRAPHICAL ABSTRACT

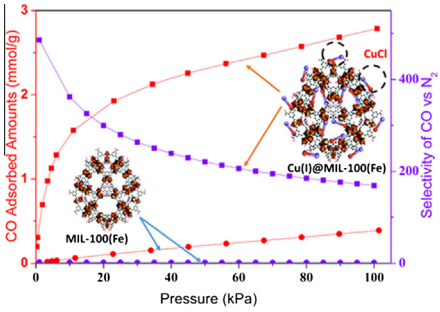

ARTICLE INFO

Article history:
Received 8 December 2014
Received in revised form 28 January 2015
Accepted 29 January 2015
Available online 7 February 2015

Keywords:
CO/N_2 separation
Cu(I)@MIL-100(Fe)
Selectivity
Adsorption

ABSTRACT

A supported Cu(I)@MIL-100(Fe) adsorbent was developed for the separation of CO/N_2 binary gas mixture. The Cu(I)@MIL-100(Fe) was prepared by the wetness impregnation of the divalent copper salts on MIL-100(Fe), followed by the reduction of $Cu^{2+} \rightarrow Cu^{+}$ under vacuum at elevated temperature. The samples were characterized by N_2 adsorption, X-ray diffraction (XRD), X-ray photoelectron spectroscopy (XPS) and Fourier transform infrared spectroscopy (FTIR). The adsorption isotherms of CO and N_2 on Cu(I)@-MIL-100(Fe) were measured by the volumetric method, and the CO/N_2 adsorption selectivities of the samples were calculated based on ideal adsorbed solution theory (IAST). The results showed that (a) the Cu(I)@MIL-100(Fe) adsorbent achieved a superior CO adsorption capacity of 2.78 mmol/g at 298 K and 100 kPa, 7 times of that on parent MIL-100(Fe), and the adsorption behavior was well described by the dual-site Langmuir–Freundlich model; (b) the CO/N_2 adsorption selectivity of Cu(I)@MIL-100(Fe) was up to 169 at 100 kPa, being 112 times of that of parent MIL-100(Fe); (c) the significant enhancement of CO uptake and CO/N_2 selectivity can be mainly attributed to the selective π-complexation between CO and Cu(I) on Cu(I)@MIL-100(Fe).

1. Introduction

As a valuable resource in chemical industry, carbon monoxide (CO) has been used as a significant fuel constituent for the production of methane, phosgene, acetic acid, formic acid, dimethyl formamide, etc. [1,2]. Generally, large quantity of CO is produced as a byproduct in tail gases from various industrial oxidation processes such as yellow phosphorus tail gas, calcium carbide furnace gas, carbon black tail gas, coke oven gas, blast furnace gas, etc. Only in China, about 15 million tons of CO is produced in steel-manufacturing process annually, which could be recycled as an inexpensive industrial raw material [3]. However, in effluent gases, CO is generally mixed with other gases such as N_2 [2,4], and thus it is imperative to separate CO from tail gases before further utilization. On the

* Corresponding authors. Tel./fax: +86 20 87113513 (J. Xiao). Tel./fax: +86 20 87110608 (Z. Li).
E-mail addresses: cejingxiao@scut.edu.cn (J. Xiao), cezhli@scut.edu.cn (Z. Li).

http://dx.doi.org/10.1016/j.cej.2015.01.126
1385-8947/

other hand, atmospheric CO is highly toxic to human because CO can bind rapidly to hemoglobin, and hinders the transportation and release of oxygen in blood [5]. In addition, even trace amount of CO has a highly adverse effect on noble metal catalysts like the platinum catalyst for hydrogen fuel cells [6,7]. Therefore, the separation and purification of CO from gas mixtures has become highly important to satisfy the industry needs and the requirement of environment protection.

Among the current CO separation and purification technologies, adsorption provides a cost-effective and eco-friendly option [1,8]. For adsorption-based separation, adsorbent is the core that directly determines the separation performance [9,10]. The reported CO adsorbents include zeolites [11,12], activated carbons [13–15], metal-supported adsorbents [8], and metal ion-based adsorbents [16–18]. Besides these conventional adsorbents, an emerging class of porous materials, metal organic frameworks (MOFs) have shown great advantages for gas adsorption and separation due to their large surface area, controllable porosity and adjustable surface properties [19–23]. The CO adsorption performance of a few MOFs has been investigated. Saha et al. [24] studied adsorption equilibria and kinetics of CO on MOF-177, and reported that it showed a higher adsorption capacity of CO than zeolite 5A and 13X at 194.5 K. Chavan et al. [25] studied CO adsorption over a microporous MOF-74(Ni), and reported that Ni^{2+} site on the 3D honeycomb network of CPO-27(Ni) was able to coordinate CO strongly at room temperature. Recently, Bloch et al. [26] reported that a series of MOF-74 achieved high CO uptakes between 2 and 6 mmol/g under ambient conditions. However, the sensitive framework of MOF-74 towards moisture might strongly hinder its industrial applications [27,28]. Krishna et al. [29] compared the adsorptive performance of three MOFs for $CO_2/CH_4/CO$ separation with that of NaX zeolite, and reported that although Cu-BTC showed the highest CO adsorption uptake at high pressure range (exceeds 1000 kPa), its CO_2/CH_4 and CO_2/CO selectivities were lower than that of NaX zeolite. Therefore, synthesis of new MOFs or surface modification of some MOFs is imperative for obtaining some MOFs with high CO adsorption capacity and selectivity.

π-complexation MOF adsorbents, functionalizing MOFs with d-block transition metal ions, has attracted attention for the selective separation of mixtures. Khan et al. [30] synthesized a Cu(I)/MIL-47(V) adsorbent and reported a doubled adsorption capacity of benzothiophene (BT) compared to the parent MIL-47(V). Ahmed et al. [31] prepared a CuCl/MIL-100(Cr) adsorbent for adsorptive denitrogenation of fuel, and reported that its adsorption capacities for quinline and indole increased by 9% and 15% compared to parent MIL-100(Cr). Chang et al. [32] prepared Cu^+/MIL-101 for ethylene/ethane separation, and reported that its C_2H_4/C_2H_6 selectivity was up to 8.7, much higher than that of the parent MIL-101(1.78). Li et al. [33] prepared an Ag^+/PAF-1 adsorbent, and reported its exceptionally high selectivity of 27–125 for C_2H_4/C_2H_6. The previous work demonstrated that the functionalization of MOFs to prepare π-complexation adsorbent can be an effective approach for improving the separation selectivity of MOFs and are worthy of further investigation. However, to the best of our knowledge, none π-complexation MOF sorbents for CO/N_2 separation from mixtures has been reported.

Herein, CuCl-supported MIL-100(Fe) was prepared to enhance the CO adsorption capacity and CO/N_2 selectivity. The textural properties of Cu(I)@MIL-100(Fe) were characterized by N_2 adsorption. The surface functionalities of Cu(I)@MIL-100(Fe) were characterized by X-ray powder diffraction (XRD), X-ray photoelectron spectroscopy (XPS) and Fourier transform infrared spectroscopy (FTIR). CO and N_2 adsorption isotherms over the adsorbents were carried out by a volumetric method. The CO/N_2 selectivity of the as-synthesized sample would be estimated by using Ideal adsorbed solution theory (IAST) based on single component isotherms of CO and N_2. The isosteric heat of CO adsorption over Cu(I)@MIL-100(Fe) was calculated. The mechanisms for enhanced CO adsorption uptake and CO/N_2 selectivity over Cu(I)@MIL-100(Fe) were discussed and reported.

2. Experimental

2.1. Materials

1,3,5-Benzenetricarboxylic acid (H_3BTC, 98%) and copper formate tetrahydrate ($Cu(HCOO)_2{\cdot}4H_2O$, 98%) were purchased from Alfa Chemicals. Iron powder (98%) was obtained from Tianjin Kemio Chemical Reagent Co. Ltd. Nitric acid (65–68%). N,N-dimethylmethanamide (DMF, 99.5%) and ethanol (99.7%) were provided by Guangzhou Guanghua Sci-Tech Co. Ltd. Hydrofluoric acid (40%) was purchased from Guangzhou Chemical Reagent Factory. Chloroform (99%) was obtained from Hunan Hengyang Kaixin Chemical Co. Ltd. Cupric chloride dehydrate ($CuCl_2{\cdot}2H_2O$, 99%) was purchased from Tianjin Damao Chemical Reagent Factory.

2.2. Preparation of Cu(I)@MIL-100(Fe)

MIL-100(Fe) was synthesized following the reported procedures [34]. Firstly, iron powder (0.56 g), H_3BTC (1.4 g), HNO_3 (0.42 mL), and HF (0.89 mL) were mixed in a Teflon autoclave reactor at 323 K for 15 min. Then, the autoclave was sealed in stainless steel vessels and kept at 433 K for 8 h. After that, the reactor was gradually cooled down to room temperature. The resulting slurry was mixed with 25 mL DMF under vigorous stirring in a conical flask for 2 h to remove unreacted precursors. The slurry was then filtered and the precipitate (fine orange powder) was dried under vacuum at 423 K for 12 h. The obtained powder was further purified in ethanol at 373 K and chloroform at ambient temperature. After filtration, the as-synthesized MIL-100(Fe) was dried at 333 K and then evacuated at 423 K for 12 h.

Cu(I)@MIL-100(Fe) was prepared by impregnation method. The preparation procedure was as follows. Firstly, MIL-100(Fe) was added into an aqueous solution mixing equimolar $CuCl_2$ and $Cu(HCOO)_2$, and then sonicated for 30 min. The slurry was heated in a rotary evaporator at 333 K to remove water. The obtained mixture was dried at 353 K and then activated in 423 K for 12 h under vacuum. The as-synthesized Cu(I)@MIL-100(Fe) was sealed and stored in a desiccator for use. The Cu(I) loadings on Cu(I)@MIL-100(Fe) were 0.2, 0.4, 0.6, 0.8, and 1.0 g/g. Accordingly, the Cu(I)@MIL-100(Fe) adsorbents were denoted as 0.2Cu(I)@MIL-100(Fe), 0.4Cu(I)@MIL-100(Fe), 0.6Cu(I)@MIL-100(Fe), 0.8Cu(I)@MIL-100(Fe), and 1.0Cu(I)@MIL-100(Fe), respectively.

2.3. Adsorbent characterizations

Nitrogen adsorption/desorption isotherms were measured at 77 K using a Micrometrics ASAP 2020 surface area and porosimetry analyzer. BET and Langmuir surface area were calculated using the standard Brunauer–Emmett–Teller (BET) equation and Langmuir model, respectively. The pressure ranges used for the calculations of both BET and Langmuir surface area were $0.05 < P/P_0 < 0.20$ (based on the three consistency criteria) [35]. The total pore volume was calculated based on the saturated N_2 adsorption amount at 100 kPa. The samples were evacuated at 423 K for 8 h before each measurement.

Powder X-ray diffraction (PXRD) measurements were performed on a Bruker D8 Advance X-ray diffractometer with Cu Kα1 radiation ($\lambda = 1.54056$) at 5–60° (2θ). X-ray photoelectron spectroscopy (XPS) was carried out on an Axis Ultra DLD spectrometer with Al Kα radiation at 1486.6 eV. FTIR spectroscopy

was performed on a Bruker 550 FTIR instrument equipped with a diffuse reflectance accessory including a reaction cell. Before each measurement, the samples were outgassed at 423 K for 5 h. The spectra were collected in the range of 400–4000 cm^{-1} with a resolution of 4 cm^{-1}.

2.4. Measurement of CO and N_2 adsorption isotherms

Adsorption isotherms of CO and N_2 were measured on the Micromeritics ASAP 2020 at varied temperatures and pressures up to 100 kPa using a standard static volumetric technique. The temperatures were strictly controlled by using a Dewar with a circulating jacket connected to a thermostatic bath with a precision of ±0.01 K. The free space of the system was determined by dozing the helium gas. Before each measurement, about 80 mg of the sample was degassed at 423 K in vacuum for 8 h. Ultrahigh purity grade helium (99.999%), CO (99.99%), N_2 (99.99%) were used as received without any purification.

3. Results and discussion

3.1. Characterization of Cu(I)@MIL-100(Fe)

Fig. 1 shows the N_2 adsorption isotherms of the samples at 77 K. The isotherms of the parent and CuCl-loaded MIL-100(Fe) adsorbents exhibited the typical type-I isotherms. The equilibrium adsorbed amount of N_2 was noted to decrease with an increase in the CuCl loading on MIL-100(Fe). Table 1 lists the textural properties of Cu(I)@MIL-100(Fe) adsorbents. The result indicated that the surface area and total pore volume of Cu(I)@MIL-100(Fe) decreased with the CuCl loadings, which could be attributed to the occupation of partial surface area and pore volume of MIL-100(Fe) by CuCl, similar as reported MIL-101 after loading Pd [36,37] and $CuCl_2$-loaded MIL-47(V) [30].

Fig. 2 shows the PXRD patterns of Cu(I)@MIL-100(Fe) with various CuCl loadings. The parent MIL-100(Fe) showed the characteristic peaks at 6.3°, 10.2°, 11.0°, and 20.0°, consistent with those reported in the literature [23,38], Cu(I)@MIL-100(Fe) maintained the similar characteristic peaks as MIL-100(Fe), suggesting the crystalline structure of MIL-100(Fe) was well preserved after the loading of the copper salts. In terms of the loaded copper salts on MIL-100(Fe), it can be seen that neither $CuCl_2$ nor $Cu(HCOO)_2$ were observed in the XRD patterns of Cu(I)@MIL-100(Fe). In addition, characteristic peaks of CuCl were absent in XRD patterns. This might be due to the presence of amorphous copper particles or well dispersed CuCl on the MIL-100(Fe) surface, as the crystalline size of the copper salts was beyond the detection limit of XRD [39]. A high dispersion of the copper salts on MIL-100(Fe) can be caused by the interaction between Cu(I) and the MIL-100(Fe) support, which made the Cu(I) particles tend to spread rather than agglomerate on MIL-100(Fe) surface.

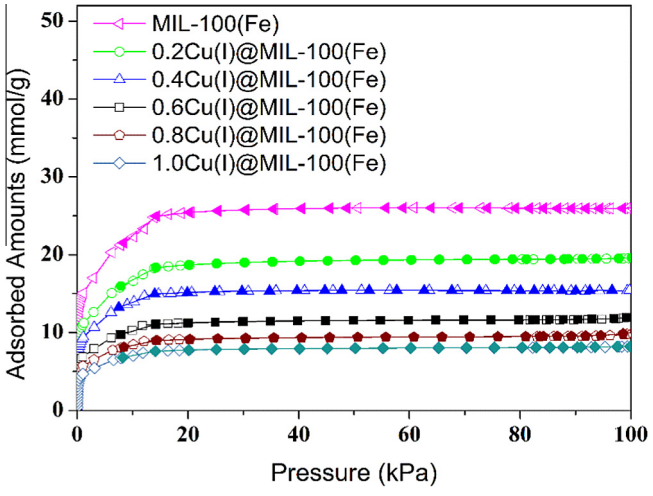

Fig. 1. N_2 adsorption isotherms of MIL-100(Fe) and Cu(I)@MIL-100(Fe) at 77 K. (The open symbols present the adsorption isotherms, and the solid symbols refer to the desorption isotherms.)

XPS was carried out to investigate the oxidation states of copper element in the Cu(I)@MIL-100(Fe) adsorbent. Fig. 3 shows the XPS spectra of the Cu(I)@MIL-100(Fe) adsorbents referred to the standard CuCl and $CuCl_2$ samples [31]. In distinct contrast, the XPS spectrum of the CuCl showed the $Cu2p_{3/2}$ peak at 932.60 eV and the $Cu2p_{1/2}$ peak at 952.2 eV, while that for the $CuCl_2$ showed the $Cu2p_{3/2}$ peak at 935.6 eV and the $Cu2p_{1/2}$ peak at 955.0 eV, accompanied with the satellite peaks at 943.4 eV and 963.8 eV. Referred to that, Cu(I)@MIL-100(Fe) sample showed the similar characteristic peaks as those for the standard Cu(I), distinguished from those for the standard Cu^{2+}. The XPS results suggested that the chemical state of the copper on Cu(I)@MIL-100(Fe) was +1 predominantly, indicating that Cu^{2+} was successfully reduced to Cu^{+} during material activation under vacuum. The absence of the satellite peaks on the XPS spectrum of the Cu(I)@MIL-100(Fe) sample further supported this assertion.

Fig. 4 shows the FTIR spectra of the Cu(I)@MIL-100(Fe) referred to the parent MIL-100(Fe). 0.8Cu(I)@MIL-100(Fe) showed highly similar IR patterns as that for MIL-100(Fe), which also matched well with those reported in the literature [40,41]. Interestingly, the peaks at 1630 cm^{-1}, characteristic of the vibrations of benzene rings, were much weaker for 0.8Cu(I)@MIL-100(Fe) than that for the parent MIL-100(Fe). The reason may be that Cu^{+} interacted with the benzene groups on the organic linker of MIL-100(Fe) through the electrostatic interaction [42,43], and thus covered the benzene sites on MIL-100(Fe) after CuCl loading, resulting in a weakened vibration signal of the benzene groups in IR spectrum.

3.2. CO and N_2 isotherms of Cu(I)@MIL-100(Fe)

Fig. 5 presents the adsorption isotherms of CO on Cu(I)@MIL-100(Fe) adsorbents with different CuCl loading. It can be seen that the Cu(I)@MIL-100(Fe) adsorbents showed significantly higher adsorption capacities compared to the original MIL-100(Fe), implying that the loading of CuCl onto the MIL-100(Fe) is an effective method to improve CO adsorption capacity significantly.

It was observed from Fig. 5(a) that the CO equilibrium uptakes of Cu(I)@MIL-100(Fe) increased with CuCl loading in the range of 0–0.8. The adsorption capacity reached a maximum value of 2.78 mmol/g. After that, a further increase in CuCl loading no longer improved CO capture capacity of Cu(I)@MIL-100(Fe). Both of CuCl loading and BET surface area of Cu(I)@MIL-100(Fe) adsorbents contributed to CO adsorption capacity. On one hand, with an increase in CuCl loading, the CO adsorption sites on Cu(I)@MIL-100(Fe) increased, which resulted in an increase in CO uptake. To get better understanding of the CuCl loading influence on the CO adsorption, the CO isotherms based on per unit mass of an adsorbent in Fig. 5(a) were converted to those based on per unit surface area, as shown in Fig. 5(b). It was found that the equilibrium uptakes of CO per unit surface area of Cu(I)@MIL-100(Fe) adsorbents were in proportion to the corresponding CuCl loading. The higher the CuCl loading was, the higher the equilibrium uptakes of CO per unit surface area of Cu(I)@MIL-100(Fe). On the other hand, an increase in CuCl loading led to a decrease in the surface area and pore volume of the adsorbents as indicated in Table 1, which would result in a decrease in CO uptake per unit mass of an adsorbent. As a result, there was an optimal CuCl loading and it was 0.8 in this study.

Table 1
Textural properties of Cu(I)@MIL-100(Fe) with various CuCl loading.

Adsorbent	BET surface area (m^2/g)	Langmuir surface area (m^2/g)	Total pore volume (cm^3/g)
MIL-100(Fe)	2042	2831	0.90
0.2Cu(I)@MIL-100(Fe)	1489	2057	0.68
0.4Cu(I)@MIL-100(Fe)	1190	1616	0.53
0.6Cu(I)@MIL-100(Fe)	886	1210	0.41
0.8Cu(I)@MIL-100(Fe)	762	1035	0.36
1.0Cu(I)@MIL-100(Fe)	610	838	0.28

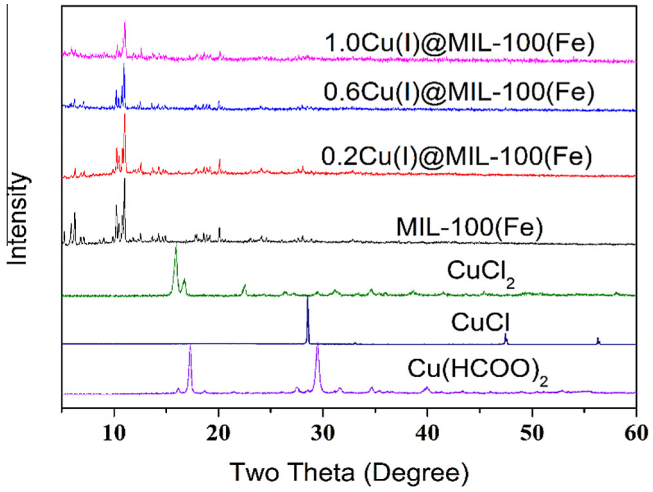

Fig. 2. PXRD patterns of Cu(I)@MIL-100(Fe) referred to MIL-100(Fe).

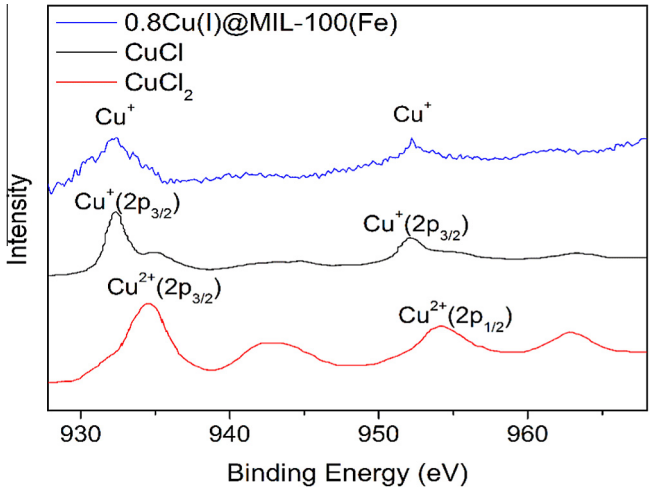

Fig. 3. XPS spectra of Cu(I)@MIL-100(Fe) referred to standard CuCl and $CuCl_2$ samples.

It was noticed that the equilibrium CO uptake of parent MIL-100(Fe) increased almost linearly with the CO pressure. In contrast to that, CO isotherms of Cu(I)@MIL-100(Fe) showed type-I isotherms, and its CO adsorption capacity showed a significant increase at low pressure. It implied that there was a relatively weak CO adsorption affinity to MIL-100(Fe), and there existed a strong adsorption affinity between CO and Cu(I)@MIL-100(Fe). In other words, the significantly enhanced CO adsorption capacity of Cu(I)@MIL-100(Fe) can be ascribed to the presence of strong CO adsorption sites of Cu(I) on the Cu(I)@MIL-100(Fe) surfaces, which can bind CO via π-complexation.

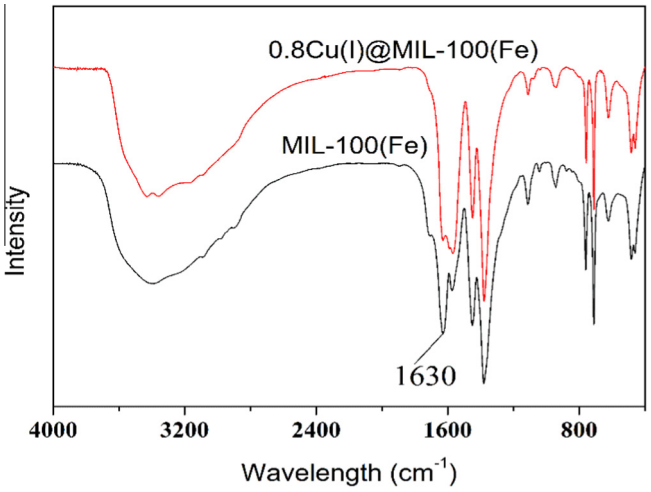

Fig. 4. FTIR spectra of Cu(I)@MIL-100(Fe) referred to MIL-100(Fe).

Table 2 summarized the CO adsorption capacities of Cu(I)@MIL-100(Fe) adsorbent and those reported in some literatures. In comparison, the 0.8Cu(I)/MIL-100(Fe) exhibited a higher CO adsorption capacity of 2.78 mmol/g than conventional adsorbents, including zeolite 5A, zeolite 13X, and AC D55/2 C PSA, and most metal organic frameworks, including MOF-5, MOF-177, HKUST-1, MIL-101(Cr), and MIL-100(Fe) from this work. The exceptional case is MOF-74(Fe), which showed a super-high CO adsorption uptake of ~6.0 mmol/g, which could be attributed to its high concentration of open metal sites that can bind CO strongly.

Fig. 6 showed N_2 adsorption isotherms of Cu(I)@MIL-100(Fe) referred to the parent MIL-100(Fe). Different from CO, the N_2 uptake decreased with the CuCl loading due to a decline in surface area and no specific interaction between Cu(I) and N_2. With a significantly enhanced CO adsorption uptake and decreased N_2 uptake after the loading of CuCl on MIL-100(Fe), it can be expected that the CO/N_2 adsorption selectivity of Cu(I)@MIL-100(Fe) could be greatly enhanced, which would be further studied and discussed next.

3.3. CO/N_2 adsorption selectivity of Cu(I)@MIL-100(Fe)

Dual-site Langmuir–Freundlich (DSLF) model was employed to describe the CO adsorption behavior on adsorbents [10,46]. The DSLF equation can be expressed as follows:

$$q = q_{m,1}\frac{b_1 p^{1/n_1}}{1 + b_1 p^{1/n_1}} + q_{m,2}\frac{b_2 p^{1/n_2}}{1 + b_2 p^{1/n_2}} \quad (1)$$

where p is the pressure of the bulk gas at equilibrium with the adsorbed phase (kPa); $q_{m,1}$ and $q_{m,2}$ are the saturation capacities of sites 1 and 2 (mmol/g); b_1 and b_2 are the affinity coefficients of sites 1 and 2 (1/kPa), respectively; n_1 and n_2 are the corresponding deviations from an ideal homogeneous surface. The DSLF model was combined with IAST to predict the adsorption isotherms of mixture and calculate the selectivity of the adsorbate.

Fig. 7 presents the CO and N_2 isotherms of 0.8Cu(I)@MIL-100(Fe) and MIL-100(Fe) fitted by the DSLF model, Table 3 lists the fitting parameters of the DSLF model. The correlation coefficients (R^2) were up to 0.9995, indicating that the adsorption behaviors of CO and N_2 on the samples can be well described by the DSLF model.

Ideal adsorbed solution theory (IAST) is widely applied to predict the adsorption selectivities of binary gas mixtures from pure component isotherms [47–49]. IAST assumes the adsorbed mixture

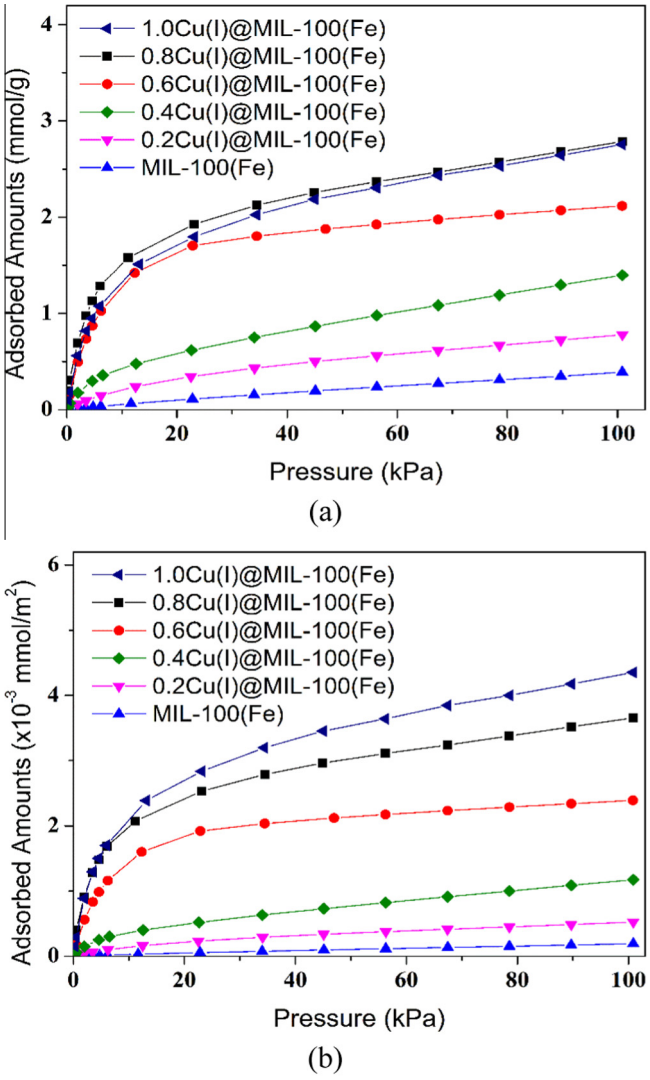

Fig. 5. CO adsorption isotherms on the samples at 298 K (a) adsorbent weight-based uptake; (b) adsorbent BET surface area-based uptake.

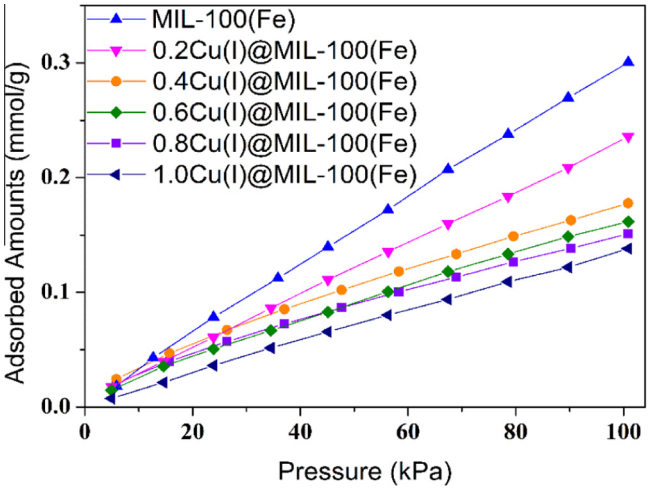

Fig. 6. N_2 isotherms of the samples at 298 K.

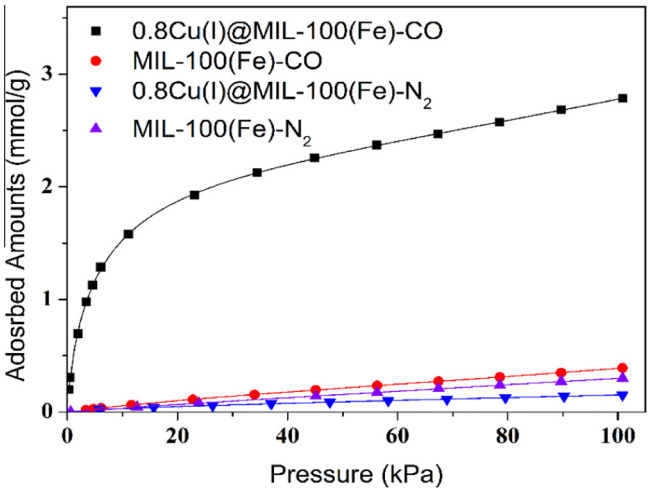

Fig. 7. CO and N_2 isotherms of Cu(I)@MIL-100(Fe) and MIL-100(Fe) at 298 K.

Table 2
CO adsorption capacities of different adsorbents at 1 bar.

Adsorbent	Adsorption capacity (mmol/g)	Temperature (K)	Reference
Zeolite 5A	~1.2	298	[24]
Zeolite 13X	~0.5	298	[24]
AC D55/2 C PSA	~0.75	298	[13]
MOF-5	~0.15	298	[24]
MOF-177	~0.03	298	[24]
HKUST-1	~0.75	295	[44]
MIL-101(Cr)	1.13	288	[45]
MOF-74(Fe)	6.04	298	[26]
MIL-100(Fe)	0.38	298	This work
0.8Cu(I)@MIL-100(Fe)	2.78	298	This work

is an ideal solution at constant spreading pressure and temperature, where the chemical potential of the adsorbed solution is considered to be equal to that of the gas phase at equilibrium [50].

Figs. 8 and 9 show the IAST-predicted adsorption isotherms for equimolar mixtures of CO/N_2 on the samples MIL-100(Fe) and 0.8Cu(I)@MIL-100(Fe), respectively, as functions of the total bulk pressure. It was clearly visible from Fig. 8 that in comparison with N_2, CO was preferentially adsorbed on MIL-100(Fe) over N_2 due to its higher polarizability (19.5 vs $17.4 \times 10^{-25}/cm^3$), dipole moment (0.11 vs 0×10^{-8}/esu cm) and quadruple moment (2.50 vs 1.52×10^{-26}/esu cm^2) [19]. Furthermore, CO adsorption capacity of Cu(I)@MIL-100(Fe) was improved significantly due to loading Cu(I) in comparison with MIL-100(Fe), which can be ascribed to π-complexation between Cu(I) and CO. Meanwhile, the N_2 uptake on 0.8Cu(I)@MIL-100(Fe) was almost negligible without such strong interaction, as shown in Fig. 9.

Fig. 10 presents the IAST-predicted CO/N_2 adsorption selectivities of two samples for equimolar CO and N_2 mixtures at 298 K as functions of the total bulk pressure. The CO/N_2 selectivity of 0.8Cu(I)@MIL-100(Fe) was much higher than that of MIL-100(Fe) in the whole measured pressure range. It decreased gradually with an increase in pressure. However, even at 100 kPa, the CO/N_2 adsorption selectivity of 0.8Cu(I)@MIL-100(Fe) was still up to 169, whereas that of the parent MIL-100(Fe) was only about 1.5. The former was about 112 times of that of MIL-100(Fe).

3.4. Isosteric heat of adsorption

Isosteric heat of adsorption is one critical thermodynamic parameter to evaluate the interaction between an adsorbate and an

Table 3
Fitting parameters and correlation coefficients of the DSLF isotherms.

Parameters	MIL-100(Fe)		0.8Cu(I)@MIL-100(Fe)	
	CO	N_2	CO	N_2
$q_{m,1}$	8.718	9.526	7.833	8.009
b_1	3.340×10^{-4}	1.666×10^{-4}	1.004×10^{-5}	8.165×10^{-4}
n_1	1.068	1.034	0.532	1.604
$q_{m,2}$	4.153	4.0135	2.63273	2.92373
b_2	1.120×10^{-3}	5.1009×10^{-4}	2.226×10^{-1}	4.37284×10^{-5}
n_2	1.264	1.041	1.269	0.814
R^2	0.9998	0.9997	0.9998	0.9999

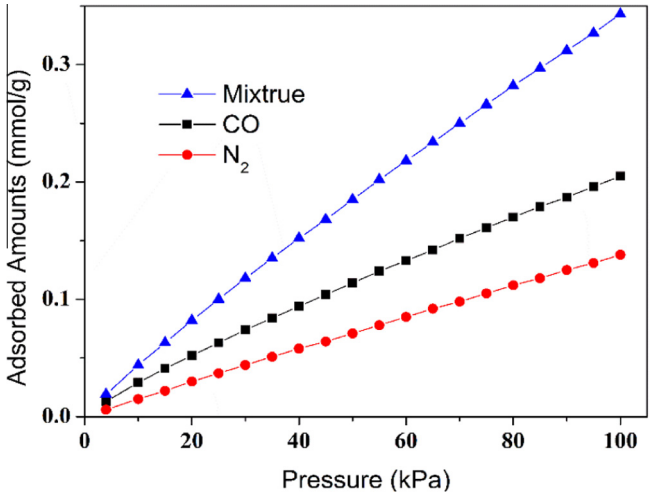

Fig. 8. IAST-predicted isotherms for equimolar CO/N_2 mixtures on MIL-100(Fe) at 298 K.

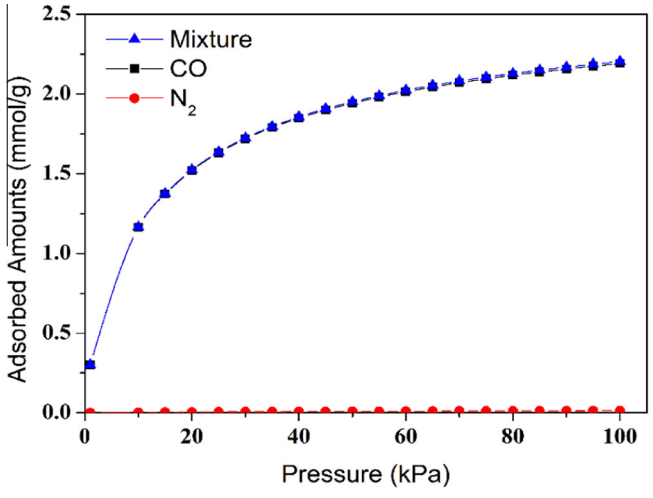

Fig. 9. IAST-predicted isotherms for equimolar CO/N_2 mixtures on 0.8Cu(I)@MIL-100(Fe) at 298 K.

adsorbent [51]. The isosteric heat of adsorption can be calculated using Clausius–Clapeyron equation as:

$$\ln P = -\frac{\Delta H_s}{RT} + C \quad (2)$$

where P is the pressure, R is the ideal gas constant, T is the absolute temperature and C is the constant. Therefore, ΔH_s can be derived from the slopes of plots of $\ln P$ versus $1/T$ of constant loading. The

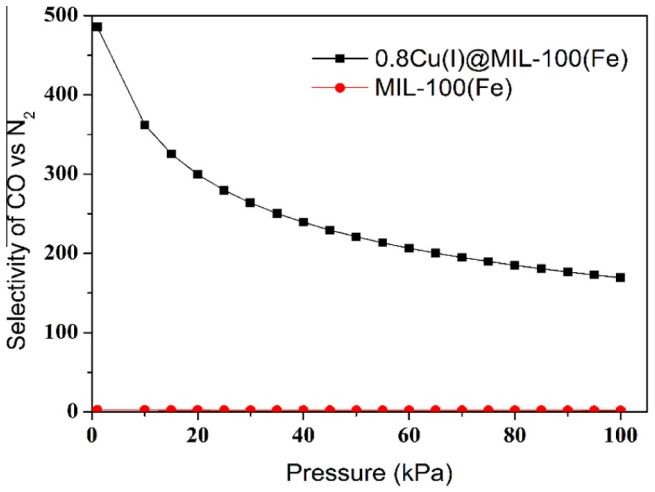

Fig. 10. IAST-predicted selectivities for equimolar CO/N_2 mixtures on 0.8Cu(I)@MIL-100(Fe) at 298 K.

partial pressure for different temperatures at fixed adsorption capacity can be calculated from the fitted DSLF equations.

Fig. 11 presents the experimental isotherms and the DSLF equation predicted isotherms of CO on 0.8Cu(I)@MIL-100(Fe) and the parent MIL-100(Fe) separately at 288 K, 298 K and 308 K. The isosteric heat of CO adsorption was derived from the fitted DSLF equation, as shown in Fig. 12. It showed that the initial isosteric heat of CO adsorption on the parent MIL-100(Fe) was about 38 kJ/mol, and then it dropped sharply with amount adsorbed of CO. For 0.8Cu(I)@MIL-100(Fe), its isosteric heats of CO adsorption were higher than those on MIL-100(Fe), suggesting that 0.8Cu(I)@MIL-100(Fe) has stronger interaction with CO than MIL-100(Fe). In addition, the isosteric heats of CO on 0.8Cu(I)@MIL-100(Fe) basically remained around 50 kJ/mol in the whole pressure range, which was also similar to the isosteric heat of CO adsorption on the pure CuCl (between the experimental and theoretical ΔH_s) [52]. It meant that the loading of CuCl on MIL-100(Fe) was helpful to make the surface force field toward CO of Cu(I)@MIL-100(Fe) more homogeneous compared to MIL-100(Fe).

4. Conclusions

A novel Cu(I)@MIL-100(Fe) adsorbent was synthesized by the wetness impregnation of the divalent copper salts onto MIL-100(Fe), followed by the reduction of $Cu^{2+} \rightarrow Cu^{+}$ under vacuum at elevated temperature. The XPS and XRD characterizations showed that the impregnated cupric salts on MIL-100(Fe) were successfully reduced to cuprous salts. CO adsorption capacities of Cu(I)@MIL-100(Fe) samples were obviously higher than that of MIL-100(Fe), and increased sharply with the CuCl loading. The CO adsorption capacity of 0.8Cu(I)@MIL-100(Fe) reached 2.78 mmol/g, being about 7 times that of the parent MIL-100(Fe). Meanwhile, its N_2 capacity became lower compared to MIL-100(Fe). As a result, the CO/N_2 selectivity of 0.8Cu(I)@MIL-100(Fe) was greatly higher than that of MIL-100(Fe) in the whole measured pressure range. It decreased gradually with pressure. It was noteworthy that even at 100 kPa, the CO/N_2 adsorption selectivity of 0.8Cu(I)@MIL-100(Fe) was still up to 169, whereas that of the parent MIL-100(Fe) was only about 1.5. The former was about 112 times of that of MIL-100(Fe). The high CO adsorption capacity and CO/N_2 selectivity can be attributed to the strong π-complexation between Cu(I)@MIL-100(Fe) and CO with an isosteric heat of adsorption ~50 kJ/mol. These excellent adsorption properties of 0.8Cu(I)@MIL-100(Fe) with high CO adsorption

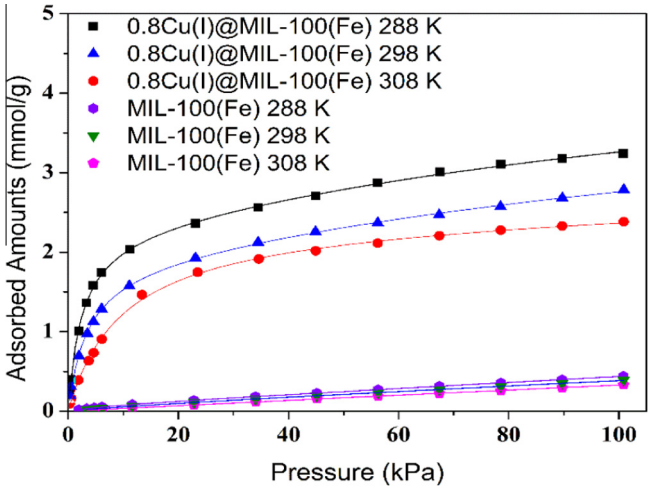

Fig. 11. CO adsorption isotherms of the samples at 288 K, 298 K and 308 K.

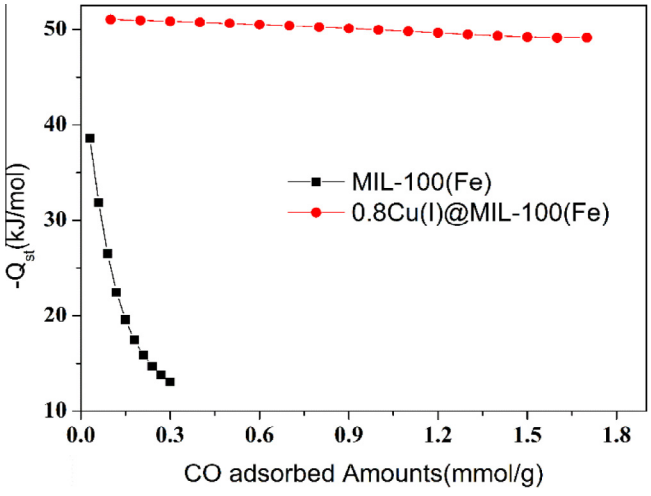

Fig. 12. Isosteric heat of MIL-100(Fe) and 0.8Cu(I)@MIL-100(Fe).

capacity and CO/N_2 selectivity would make it become a promising adsorbent for the effective separation of CO/N_2.

Acknowledgements

This work was supported by National Key Basic Research Program of China (No. 2013CB733506), National Science Fund for Distinguished Young Scholars of China (No. 21225625), National Natural Science Foundation of China (No. 21276092), the Research Foundation of State Key Lab of Subtropical Building Science of China (No. C713001z), and the Fundamental Research Funds for the Central Universities.

Appendix A. Supplementary data

Supplementary data associated with this article can be found, in the online version, at http://dx.doi.org/10.1016/j.cej.2015.01.126.

References

[1] Y. Xie, J. Zhang, J. Qiu, X. Tong, J. Fu, G. Yang, H. Yan, Y. Tang, Zeolites modified by CuCl for separating CO from gas mixtures containing CO_2, Adsorption 3 (1997) 27–32.
[2] G. Zarca, I. Ortiz, A. Urtiaga, Copper(I)-containing supported ionic liquid membranes for carbon monoxide/nitrogen separation, J. Membr. Sci. 438 (2013) 38–45.
[3] L. Wang, Q. Zhang, J. Hao, K. He, Anthropogenic CO emission inventory of Mainland China, Acta Sci. Circum. 25 (2005) 1580–1585.
[4] H. Sato, W. Kosaka, R. Matsuda, A. Hori, Y. Hijikata, R.V. Belosludov, S. Sakaki, M. Takata, S. Kitagawa, Self-accelerating CO sorption in a soft nanoporous crystal, Science 343 (2014) 167–170.
[5] J.B. DeCoste, G.W. Peterson, Metal–organic frameworks for air purification of toxic chemicals, Chem. Rev. 114 (2014) 5695–5727.
[6] C. Bonnet, L. Franck-Lacaze, S. Ronasi, S. Besse, F. Lapicque, PEM fuel cell Pt anode inhibition by carbon monoxide: non-uniform behaviour of the cell caused by the finite hydrogen excess, Chem. Eng. Sci. 65 (2010) 3050–3058.
[7] X. Cheng, Z. Shi, N. Glass, L. Zhang, J. Zhang, D. Song, Z.-S. Liu, H. Wang, J. Shen, A review of PEM hydrogen fuel cell contamination: impacts, mechanisms, and mitigation, J. Power Sources 165 (2007) 739–756.
[8] L. Wang, J. Zhao, L. Wang, T. Yan, Y.-Y. Sun, S.B. Zhang, Titanium-decorated graphene oxide for carbon monoxide capture and separation, Phys. Chem. Chem. Phys. 13 (2011) 21126–21131.
[9] R.T. Yang, Adsorbents: Fundamentals and Applications, John Wiley & Sons, 2003.
[10] W. Huang, X. Zhou, Q. Xia, J. Peng, H. Wang, Z. Li, Preparation and adsorption performance of GrO@Cu-BTC for separation of CO_2/CH_4, Ind. Eng. Chem. Res. 53 (2014) 11176–11184.
[11] K. Chakarova, K. Hadjiivanov, H-bonding of zeolite hydroxyls with weak bases: FTIR study of CO and N_2 adsorption on HD-ZSM-5, J. Phys. Chem. C 115 (2011) 4806–4817.
[12] M.R. Delgado, C.O. Arean, Carbon monoxide, dinitrogen and carbon dioxide adsorption on zeolite H-beta: IR spectroscopic and thermodynamic studies, Energy 36 (2011) 5286–5291.
[13] M. Bastos-Neto, A. Moeller, R. Staudt, J. Böhm, R. Gläser, Dynamic bed measurements of CO adsorption on microporous adsorbents at high pressures for hydrogen purification processes, Sep. Purif. Technol. 77 (2011) 251–260.
[14] C.A. Grande, F.V. Lopes, A.M. Ribeiro, J.M. Loureiro, A.E. Rodrigues, Adsorption of off-gases from steam methane reforming (H_2, CO_2, CH_4, CO and N_2) on activated carbon, Sep. Sci. Technol. 43 (2008) 1338–1364.
[15] F.V. Lopes, C.A. Grande, A.M. Ribeiro, J.M. Loureiro, O. Evaggelos, V. Nikolakis, A.E. Rodrigues, Adsorption of H_2, CO_2, CH_4, CO, N_2 and H_2O in activated carbon and zeolite for hydrogen production, Sep. Sci. Technol. 44 (2009) 1045–1073.
[16] X. Zheng, Y. Zhang, A.T. Bell, Density functional theory study of CO adsorption on Cu(I)-ZSM-5, J. Phys. Chem. C 111 (2007) 13442–13451.
[17] J. Ma, L. Li, J. Ren, R. Li, CO adsorption on activated carbon-supported Cu-based adsorbent prepared by a facile route, Sep. Purif. Technol. 76 (2010) 89–93.
[18] Y. Yin, P. Tan, X.-Q. Liu, J. Zhu, L.-B. Sun, Constructing a confined space in silica nanopores: an ideal platform for the formation and dispersion of cuprous sites, J. Mater. Chem. A 2 (2014) 3399–3406.
[19] J.-R. Li, R.J. Kuppler, H.-C. Zhou, Selective gas adsorption and separation in metal–organic frameworks, Chem. Soc. Rev. 38 (2009) 1477–1504.
[20] X. Zhou, W. Huang, J. Miao, Q. Xia, Z. Zhang, H. Wang, Z. Li, Enhanced separation performance of a novel composite material GrO@MIL-101 for CO_2/CH_4 binary mixture, Chem. Eng. J. 266 (2014) 339–344.
[21] F. Raganati, V. Gargiulo, P. Ammendola, M. Alfe, R. Chirone, CO_2 capture performance of HKUST-1 in a sound assisted fluidized bed, Chem. Eng. J. 239 (2014) 75–86.
[22] L. Xie, D. Liu, H. Huang, Q. Yang, C. Zhong, Efficient capture of nitrobenzene from waste water using metal–organic frameworks, Chem. Eng. J. 246 (2014) 142–149.
[23] P.-J. Kim, Y.-W. You, H. Park, J.-S. Chang, Y.-S. Bae, C.-H. Lee, J.-K. Suh, Separation of SF_6 from SF_6/N_2 mixture using metal–organic framework MIL-100(Fe) granule, Chem. Eng. J. 262 (2014) 683–690.
[24] D. Saha, S. Deng, Adsorption equilibria and kinetics of carbon monoxide on zeolite 5A, 13X, MOF-5, and MOF-177, J. Chem. Eng. Data 54 (2009) 2245–2250.
[25] S. Chavan, J.G. Vitillo, E. Groppo, F. Bonino, C. Lamberti, P.D. Dietzel, S. Bordiga, CO adsorption on CPO-27-Ni coordination polymer: spectroscopic features and interaction energy, J. Phys. Chem. C 113 (2009) 3292–3299.
[26] E.D. Bloch, M.R. Hudson, J.A. Mason, S. Chavan, V. Crocellà, J.D. Howe, K. Lee, A.L. Dzubak, W.L. Queen, J.M. Zadrozny, Reversible CO binding enables tunable CO/H_2 and CO/N_2 separations in metal–organic frameworks with exposed divalent metal cations, J. Am. Chem. Soc. 136 (2014) 10752–10761.
[27] J.B. DeCoste, G.W. Peterson, B.J. Schindler, K.L. Killops, M.A. Browe, J.J. Mahle, The effect of water adsorption on the structure of the carboxylate containing metal–organic frameworks Cu-BTC, Mg-MOF-74, and UiO-66, J. Mater. Chem. A 1 (2013) 11922–11932.
[28] A.C. Kizzie, A.G. Wong-Foy, A.J. Matzger, Effect of humidity on the performance of microporous coordination polymers as adsorbents for CO_2 capture, Langmuir 27 (2011) 6368–6373.
[29] R. Krishna, Adsorptive separation of $CO_2/CH_4/CO$ gas mixtures at high pressures, Microporous Mesoporous Mater. 156 (2012) 217–223.
[30] N.A. Khan, S.H. Jhung, Remarkable adsorption capacity of $CuCl_2$-loaded porous vanadium benzenedicarboxylate for benzothiophene, Angew. Chem. 124 (2012) 1224–1227.
[31] I. Ahmed, S.H. Jhung, Adsorptive denitrogenation of model fuel with CuCl-loaded metal–organic frameworks (MOFs), Chem. Eng. J. 251 (2014) 35–42.

[32] G. Chang, Z. Bao, Q. Ren, S. Deng, Z. Zhang, B. Su, H. Xing, Y. Yang, Fabrication of cuprous nanoparticles in MIL-101: an efficient adsorbent for the separation of olefin–paraffin mixtures, RSC Adv. 4 (2014) 20230–20233.
[33] B. Li, Y. Zhang, R. Krishna, K. Yao, Y. Han, Z. Wu, D. Ma, Z. Shi, T. Pham, B. Space, Introduction of π-complexation into porous aromatic framework for highly selective adsorption of ethylene over ethane, J. Am. Chem. Soc. 136 (2014) 8654–8660.
[34] J.W. Yoon, Y.K. Seo, Y.K. Hwang, J.S. Chang, H. Leclerc, S. Wuttke, P. Bazin, A. Vimont, M. Daturi, E. Bloch, Controlled reducibility of a metal–organic framework with coordinatively unsaturated sites for preferential gas sorption, Angew. Chem. Int. Ed. 49 (2010) 5949–5952.
[35] K.S. Walton, R.Q. Snurr, Applicability of the BET method for determining surface areas of microporous metal–organic frameworks, J. Am. Chem. Soc. 129 (2007) 8552–8556.
[36] H. Li, Z. Zhu, F. Zhang, S. Xie, H. Li, P. Li, X. Zhou, Palladium nanoparticles confined in the cages of MIL-101: an efficient catalyst for the one-pot indole synthesis in water, ACS Catal. 1 (2011) 1604–1612.
[37] Y. Pan, B. Yuan, Y. Li, D. He, Multifunctional catalysis by Pd@MIL-101: one-step synthesis of methyl isobutyl ketone over palladium nanoparticles deposited on a metal–organic framework, Chem. Commun. 46 (2010) 2280–2282.
[38] S.-H. Huo, X.-P. Yan, Metal–organic framework MIL-100(Fe) for the adsorption of malachite green from aqueous solution, J. Mater. Chem. 22 (2012) 7449–7455.
[39] Y. Chen, C. Xie, Y. Li, C. Song, T.B. Bolin, Sulfur poisoning mechanism of steam reforming catalysts: an X-ray absorption near edge structure (XANES) spectroscopic study, Phys. Chem. Chem. Phys. 12 (2010) 5707–5711.
[40] R. Canioni, C. Roch-Marchal, F. Sécheresse, P. Horcajada, C. Serre, M. Hardi-Dan, G. Férey, J.-M. Grenèche, F. Lefebvre, J.-S. Chang, Stable polyoxometalate insertion within the mesoporous metal organic framework MIL-100 (Fe), J. Mater. Chem. 21 (2011) 1226–1233.
[41] G. Song, Z. Wang, L. Wang, G. Li, M. Huang, F. Yin, Preparation of MOF(Fe) and its catalytic activity for oxygen reduction reaction in an alkaline electrolyte, Chin. J. Catal. 35 (2014) 185–195.
[42] J. Xiao, X. Wang, M. Fujii, Q. Yang, C. Song, A novel approach for ultra-deep adsorptive desulfurization of diesel fuel over TiO_2–CeO_2/MCM-48 under ambient conditions, AIChE J. 59 (2013) 1441–1445.
[43] J. Xiao, C. Song, X. Ma, Z. Li, Effects of aromatics, diesel additives, nitrogen compounds, and moisture on adsorptive desulfurization of diesel fuel over activated carbon, Ind. Eng. Chem. Res. 51 (2012) 3436–3443.
[44] Q. Min Wang, D. Shen, M. Bülow, M. LingLau, S. Deng, F.R. Fitch, N.O. Lemcoff, J. Semanscin, Metallo-organic molecular sieve for gas separation and purification, Microporous Mesoporous Mater. 55 (2002) 217–230.
[45] K. Munusamy, G. Sethia, D.V. Patil, P.B. Somayajulu Rallapalli, R.S. Somani, H.C. Bajaj, Sorption of carbon dioxide, methane, nitrogen and carbon monoxide on MIL-101(Cr): volumetric measurements and dynamic adsorption studies, Chem. Eng. J. 195 (2012) 359–368.
[46] T.F.d. Oliveira, E.S. Ribeiro, M.G. Segatelli, C.R.T. Tarley, Enhanced sorption of Mn^{2+} ions from aqueous medium by inserting protoporphyrin as a pendant group in poly(vinylpyridine) network, Chem. Eng. J. 221 (2013) 275–282.
[47] Y. Li, H. Yi, X. Tang, F. Li, Q. Yuan, Adsorption separation of CO_2/CH_4 gas mixture on the commercial zeolites at atmospheric pressure, Chem. Eng. J. 229 (2013) 50–56.
[48] Z. Zhao, S. Wang, Y. Yang, X. Li, J. Li, Z. Li, Competitive adsorption and selectivity of benzene and water vapor on the microporous metal organic frameworks (HKUST-1), Chem. Eng. J. 259 (2015) 79–89.
[49] N. Magnowski, A. Avila, C. Lin, M. Shi, S. Kuznicki, Extraction of ethane from natural gas by adsorption on modified ETS-10, Chem. Eng. Sci. 66 (2011) 1697–1701.
[50] A. Myers, J.M. Prausnitz, Thermodynamics of mixed-gas adsorption, AIChE J. 11 (1965) 121–127.
[51] S. Xian, X. Li, F. Xu, Q. Xia, Z. Li, Adsorption isotherms, kinetics, and desorption of 1,2-dichloroethane on chromium-based metal organic framework MIL-101, Sep. Sci. Technol. 48 (2013) 1479–1489.
[52] H.Y. Huang, J. Padin, R.T. Yang, Comparison of π-complexations of ethylene and carbon monoxide with Cu(I) and Ag^+, Ind. Eng. Chem. Res. 38 (1999) 2720–2725.